IL NUOVO CIMENTO **49 C** (2026) 112
DOI 10.1393/ncc/i2026-26112-6

Colloquia: MAYORANA 2025

Lead-induced calibration of BULLKID detector

M. Folcarelli(1)(2), A. Acevedo-Rentería(3), L. E. Ardila-Perez(4),
L. Bandiera(5), M. Calvo(6), M. Cappelli(1)(2), R. Caravita(7), F. Carillo(8),
U. Chowdhury(6), D. Crovo(4), A. Cruciani(2), A. D'Addabbo(9),
D. Delicato(6)(1)(2), M. De Lucia(10)(8), G. Del Castello(2),
M. del Gallo Roccagiovine(1)(2), F. Ferraro(9), S. Fu(9), R. Gartmann(4),
M. Grassi(8), V. Guidi(11)(5), D. Helis(9), T. Lari(10)(8), L. Malagutti(5),
A. Mazzolari(11)(5), A. Monfardini(6), T. Muscheid(4), D. Nicolò(10)(8),
F. Paolucci(10)(8), D. Pasciuto(2), L. Pesce(1)(2), C. Puglia(8),
D. Quaranta(1)(2), C. M. A. Roda(10)(8), S. Roddaro(10)(8), M. Romagnoni(5),
G. Signorelli(10)(8), F. Simon(4), A. Tartari(8), E. Vázquez-Jáuregui(3),
M. Vignati(1)(2) and K. Zhao(9)(12)

(1) *Dipartimento di Fisica, Sapienza Università di Roma - P. le A. Moro 2, 00185 Roma, Italy*
(2) *INFN Sezione di Roma - P.le A. Moro 2, 00185 Roma, Italy*
(3) *Instituto de Física, Universidad Nacional Autónoma de México - A.P. 20-364, Ciudad de México 01000, Mexico*
(4) *Institute for Data Processing and Electronics, Karlsruhe Institute of Technology Hermann-von-Helmholtz-Platz 1 76344, Eggenstein-Leopoldshafen, Germany*
(5) *INFN Sezione di Ferrara - Via Saragat 1, 44122 Ferrara, Italy*
(6) *University Grenoble Alpes, CNRS, Grenoble INP, Institut Néel - 38000 Grenoble, France*
(7) *INFN-TIFPA - Via Sommarive 14, 38123 Povo (Trento), Italy*
(8) *INFN Sezione di Pisa - Largo Bruno Pontecorvo 3, 56127 Pisa, Italy*
(9) *INFN Laboratori Nazionali del Gran Sasso - 67100 Assergi (AQ), Italy*
(10) *Dipartimento di Fisica "Enrico Fermi", Università di Pisa - Largo Bruno Pontecorvo 3, 56127 Pisa, Italy*
(11) *Dipartimento di Fisica e Scienze della Terra, Università di Ferrara - Via Saragat 1, 44100 Ferrara, Italy*
(12) *Gran Sasso Science Institute - Viale Francesco Crispi, 7, 67100 L'Aquila (AQ), Italy*

received 15 April 2026

Summary. — BULLKID-DM is an experiment designed for the direct searches of particle dark matter candidates with mass around 1 GeV, or below. It consists of a stack of diced silicon wafers, acting as arrays of particle absorbers, sensed by multiplexed Kinetic Inductance Detectors. In spring 2025, the BULLKID-DM experiment carried out a background measurement of a single detector in a mildly lead-shielded environment. The goal was to reduce the background rate below 10^5 counts/(keV kg d). Additionally, the shield produced several calibration peaks in the detector, originating from fluorescence X-rays and gamma emissions induced by ^{210}Pb contamination. In this work, we present a detailed analysis of these peaks, focusing on the calibration of the detector during the background data acquisition.

1. – Introduction

BULLKID-DM is an experiment designed for the direct search of particle dark matter candidates with masses around or below 1 GeV. It is based on BULLKID detectors [1-3], which are monolithic arrays of 5.4 × 5.4 × 5.0 mm^3 silicon dice, each instrumented with phonon-mediated cryogenic Kinetic Inductance Detectors (KIDs) [4]. In spring 2025, the collaboration performed a background measurement of a detector operated in a mildly lead-shielded environment, with the goal of reducing the background rate below 10^5 counts/(keV kg d). The shielding also produced several calibration peaks in the energy spectrum, originating from fluorescence X-rays and gamma emissions induced by ^{210}Pb contamination. These peaks enabled the evaluation of the KID response function throughout the entire data-taking period, thus providing an independent method for the detector calibration. The standard calibration approach adopted by the collaboration, in fact, relies on bursts of optical photons emitted by LED sources [5]. However, a recent study [6] using the 59.5 keV gamma line from a ^{241}Am source, revealed systematic differences in this method that are not yet fully understood. Here we present the analysis of the calibration peaks of lead and the results of the comparison with the standard optical calibration.

2. – Description

The BULLKID detector exploited in this measurement is the same adopted in [6], placed inside the lead pot shown in fig. 1 and anchored to the coldest point of a dry ^{3}He/^{4}He dilution refrigerator with base temperature of 20 mK. Additionally a lead castle around the cryostat is built to shield from the external radioactivity. The standard energy calibration is performed by shining controlled photon bursts to KID 47 and 49, dubbed as "main", on the opposite side of the lithography. The photons are produced by a room temperature 400 nm LED driver and delivered through optical fibers. The triggered data are processed offline with the matched filter and the signal amplitude is estimated as the maximum of the filtered waveform. During the entire acquisition, several optical calibrations [6, 7] are conducted to asses the response function of the main KIDs. In the following, the "LED calibrated energy" denotes the calibrated amplitude with the standard optical calibration. After applying the analysis strategy reported in [2], we reconstruct the energy spectra of the main KIDs. Figure 2 (top-left) shows such energy spectrum for KID 49 in the energy range $[2, 100]$ keV where lead peaks are clearly reconstructed and identified. A fit with a linear decreasing background and a Gaussian

Fig. 1. – Schemes and pictures of the experimental setup consisting of a lead castle and lead pot that hosts the BULLKID detector.

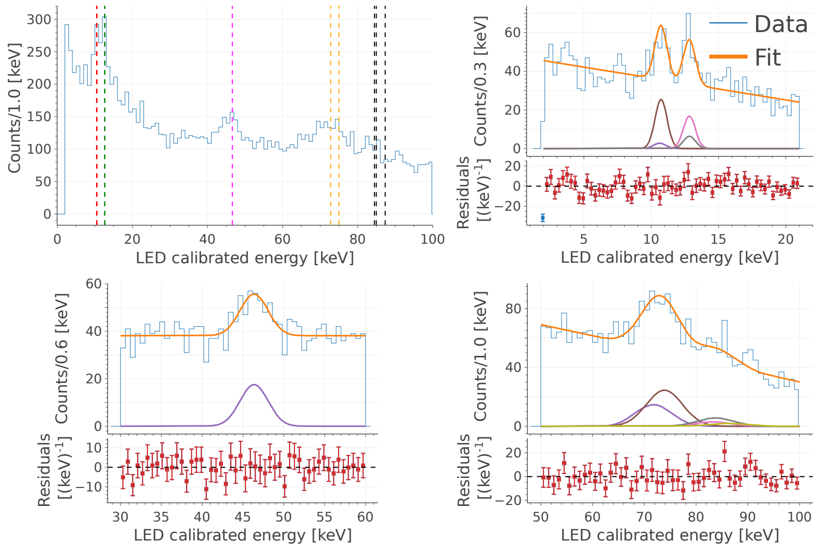

Fig. 2. – Top left: energy spectrum of KID 49, optically calibrated, in the energy range $[2, 100]$ keV. The vertical colored lines represents the nominal energies listed in table I. Others: fit of the energy spectrum in the energy ranges $[2, 21]$, $[30, 60]$ and $[50, 100]$ keV with a linearly decreasing background and a Gaussian for each of the lead peaks present in the energy range.

model of the peaks is superimposed to the energy spectrum for three different energy intervals: $[2, 21]$, $[30, 60]$ and $[50, 100]$ keV. For each interval, the standard deviation of the Gaussians is imposed to be the same for each peak, while the means and the amplitudes have a relative fixed value based on what is reported in table I from [8]. The parameters of the Gaussians with the nominal energy of the corresponding lead peak are listed in table I. By comparing the inferred mean of the first gaussian in each energy interval with its nominal energy, we can fit the response function of the main KIDs with a parabolic model of the form:

$$E_{\text{mean}} = a \cdot E_{\text{true}} \cdot (1 + b \cdot a \cdot E_{\text{true}}) \tag{1}$$

The fit and the results for both the main KIDs are reported in fig. 3, giving the following results:

$$a_{47} = 0.90 \pm 0.01 \qquad b_{47} = -(0.9 \pm 2.0) \cdot 10^{-4}\ \text{keV}^{-1}$$
$$a_{49} = 1.02 \pm 0.01 \qquad b_{49} = -(4.9 \pm 1.4) \cdot 10^{-4}\ \text{keV}^{-1}$$

3. – Conclusions

In this work we have presented the analysis of the calibration of a BULLKID detector with the X and γ ray peaks from lead, during the background acquisition with a mild shield. The resulting response function validates the standard optical calibration, as already done in [6], to an accuracy better than 12%. Additionally we asses that the LED calibration reduces the non-linearity of the KIDs to the level of 5% at 100 keV.

TABLE I. – *Main fluorescence lines of lead and the 46.6 keV γ line from ^{210}Pb contamination. Nominal energy and relative intensity* [8] *are listed, along with mean and standard deviation for the main KIDs, obtained from the fitting procedure in fig. 2.*

Line	nominal [keV]	Intensity	Mean 47 [keV]	σ 47 [keV]	Mean 49 [keV]	σ 49 [keV]
$L_{\alpha 2}$	10.45	11	9.2 ± 0.1	0.5 ± 0.1	10.6 ± 0.1	0.5 ± 0.1
$L_{\alpha 1}$	10.55	100	9.3 ± 0.1	-	10.7 ± 0.1	-
$L_{\beta 1}$	12.61	66	11.1 ± 0.1	-	12.8 ± 0.1	-
$L_{\beta 2}$	12.62	25	11.1 ± 0.1	-	12.8 ± 0.1	-
γ^{210}Pb	46.6	100	40.2 ± 0.5	2.0 ± 0.5	46.3 ± 0.4	1.7 ± 0.4
$K_{\alpha 2}$	72.80	60	63.5 ± 0.3	2.3 ± 0.3	71.7 ± 0.5	3.5 ± 0.5
$K_{\alpha 1}$	74.97	100	65.4 ± 0.3	-	73.9 ± 0.5	-
$K_{\beta 3}$	84.45	12	73.7 ± 0.4	-	83.2 ± 0.6	-
$K_{\beta 1}$	84.94	23	74.1 ± 0.4	-	83.7 ± 0.6	-
$K_{\beta 2}$	87.32	8	76.2 ± 0.4	-	86.1 ± 0.6	-

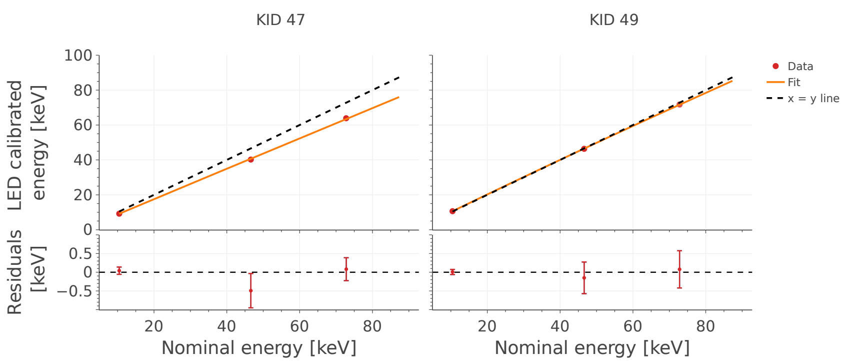

Fig. 3. – Response function of the main KIDs modeled with eq. (1). The dashed black line is the $x = y$ curve reported for reference.

* * *

This work was further supported by the INFN, Sapienza University of Rome and co-funded by the European Union (ERC, DANAE, 101087663). Views and opinions expressed are however those of the author(s) only and do not necessarily reflect those of the European Union or the European Research Council. Neither the European Union nor the granting authority can be held responsible for them.

REFERENCES

[1] CRUCIANI A.*et al.*, *Appl. Phys. Lett.*, **121** (2022) 213504.
[2] DELICATO D. *et al.*, *Eur. Phys. J. C*, **84** (2024) 4.
[3] DELICATO D. *et al.*, *Appl. Phys. Lett.*, **126** (2025) 153502.
[4] CARDANI L. *et al.*, *Eur. Phys. J. C*, **81** (2021) 636.
[5] DEL CASTELLO G., *Nucl. Instrum. Methods A*, **1068** (2024) 169728.
[6] FOLCARELLI M. *et al.*, *Energy calibration of bulk events in the BULLKID detector*, arXiv:2510.17423 (2025).
[7] CARDANI L. *et al.*, *Supercond. Sci. Technol.*, **31** (2018) 075002.
[8] THOMPSON A., *X-RAY DATA BOOKLET, Center of X-ray Optics and Advanced Light Source* (2009).